Journal of Power Sources 196 (2011) 8942–8947

Contents lists available at ScienceDirect

Journal of Power Sources

journal homepage: www.elsevier.com/locate/jpowsour

Electrolyte degradation in anode supported microtubular yttria stabilized zirconia-based solid oxide steam electrolysis cells at high voltages of operation

M.A. Laguna-Bercero[a,*], R. Campana[a], A. Larrea[a], J.A. Kilner[b], V.M. Orera[a]

[a] Instituto de Ciencia de Materiales de Aragón, ICMA, CSIC – Universidad de Zaragoza, Pedro Cerbuna 12, 50009 Zaragoza, Spain
[b] Department of Materials, Imperial College London, Prince Consort Road, SW7 2AZ London, UK

ARTICLE INFO

Article history:
Received 7 November 2010
Received in revised form
22 December 2010
Accepted 4 January 2011
Available online 15 January 2011

Keywords:
Solid oxide steam electrolyser
Hydrogen production
SOFC
SOEC
Zirconia
Microtubular

ABSTRACT

Degradation of solid oxide electrolysis cells (SOECs) is probably the biggest concern in the field of high temperature steam electrolysis (HTSE). Anode supported, YSZ-based microtubular solid oxide fuel cells (SOFC) have been tested in fuel cell mode and also at high voltages (up to 2.8 V) under electrolysis mode. At high steam conversion rates the cell voltage tends to saturate. Our hypothesis is that this effect is caused by the electroreduction of the thin YSZ electrolyte which induces electronic conduction losses. YSZ reduction increases the cathode activity and reduces cathode overpotential. Operation of the cell in severe electrolyte reduction conditions induces irreversible damage at the YSZ electrolyte as observed in SEM experiments by the formation of voids at the grain boundaries of the dense YSZ electrolyte. Evidence of this damage was also given by the increase of the ohmic resistance measured by AC impedance. Signs of electrolyte degradation were also found by both EDX analysis and micro-Raman spectroscopy performed along a transverse-cross section of the cell. The observed oxygen electrode delamination is associated to the high oxygen partial pressures gradients that take place at the electrolyte/oxygen electrode interface.

1. Introduction

In recent years, there has been a great interest in renewable energy resources, such as wind power, solar energy, hydropower or geothermal power. The main problem associated with those energies is that they have to match supply with demand, therefore energy storage is essential. Battery storage is an alternative for some applications, although they present some problems such as high costs for large storage requirements, or loss of charge overtime. Storage of H_2 will be also essential for the hydrogen economy in the near future. Hydrogen is probably the preferred energy carrier for a future zero-carbon economy but several research efforts are required in order to supply inexpensive and plentiful amounts of fuel. Water electrolysis is most likely the cleanest method to produce hydrogen [1], and at present low temperature alkaline and proton exchange membrane (PEM) electrolysers are widely used to produce zero-emission hydrogen when combined with a renewable source to supply the electricity. The problem in those systems is that >2/3 of the cost of electrolysis is due to electricity demand. By increasing the operation temperature of the electrolyser, the electrical energy demand is significantly reduced. In this area, HTSE presents particular interest as nuclear power, renewable energy and waste heat from high temperature industrial processes could be used to supply the heat and power needed for electrolysis [2]. HTSE has also attracted many researches that are trying to develop these technologies in the recent years [3–9].

Other interesting alternative for SOECs is the high temperature co-electrolysis of CO_2 and steam to produce synthesis gas [10–12]. Where a source of high temperature process heat is available, the endothermic electrolysis reactions can utilize both thermal and electrical inputs being the conversion efficiency within the cell of 100%.

Degradation of solid oxide electrolysis cells (SOECs) is possibly the largest concern in this field. For example, aging studies of metal supported cells performed at the German Aerospace Center (DLR) [4] showed a degradation rate of 3.2% per 1000 h at 800 °C, $-0.3\ A\ cm^{-2}$ and 43% of steam concentration. The degradation rate was higher than the standard for the SOFC technology. The AC impedance studies showed an enhancement in the polarization resistance during the electrolyser operation that was attributed to degradation in the hydrogen electrode. Aging studies up to 1300 h operation time at 850 °C, $-0.5\ A\ cm^{-2}$ and 50% steam, were also made at Risø-DTU National Laboratory (Denmark) showing a degradation rate of 2% [13]. They also observed by AC impedance that the degradation was mainly attributed to the Ni/YSZ electrode degradation and in fact their SEM experiments revealed grain growth of

* Corresponding author at: Instituto de Ciencia de Materiales de Aragón, ICMA, CSIC – Universidad de Zaragoza, Pedro Cerbuna 12, 50009 Zaragoza, Spain.
Tel.: +34 97676976761958; fax: +34 976761957.
E-mail address: malaguna@unizar.es (M.A. Laguna-Bercero).

0378-7753/$ – see front matter © 2011 Elsevier B.V. All rights reserved.
doi:10.1016/j.jpowsour.2011.01.015

Ni particles as well as the presence of Si impurities in all the studied samples. In contrast to these studies in a very recent study in a 720-cell stack after 1080 h of SOEC operation performed [14] the authors reported that the hydrogen electrode (Ni–YSZ) was mainly in good condition although some silicon impurities from the seal were detected. The 6ScSZ (6 mol% Sc_2O_3 stabilized zirconia) electrolyte showed no cracks or apparent grain growth although in some cases monoclinic phase was detected near the edges. The authors also claim that the biggest degradation evidences are related with the presence of Cr-doped Al_2O_3 near the seals from bipolar plates, with cation diffusion at the oxygen electrode, and with delamination of the oxygen electrode due to the high oxygen partial pressures at the electrode/electrolyte interface. Delamination of the oxygen electrode is a common problem in SOECs and has also been observed by other authors [15,16].

Those findings in the literature are also supported by the electrochemical model for degradation of solid oxide electrolyser cells recently proposed by Virkar [17]. The model showed that electronic conduction through the electrolyte must be taken into account for determining local oxygen chemical potential within the electrolyte. Under certain conditions, high oxygen pressures can develop in the electrolyte just near the oxygen electrode/electrolyte interface, leading to oxygen electrode delamination. Virkar's model also predicts that the higher the electronic conductivity of the electrolyte, the lower is the tendency for the formation of such high internal pressures. Preliminary calculations show that small changes in electronic conductivity can cause variations of orders of magnitude in the oxygen partial pressure. Thus, the study concluded that a small amount of electronic conduction through the electrolyte is preferred for the stability of the cell.

Another issue concerning SOEC operation is the degradation occurring at high current densities. Knibbe et al. [18] found that at high electrolysis current densities (>−1 A cm^{-2}), cell voltage degradation is predominately attributed to ohmic degradation and there is no direct relationship between polarization resistance degradation and current density/cell polarization.

In the present paper we report on aging studies for SOEC microtubular cells operated at high voltages. The advantages of using the microtubular configuration include easier sealings in comparison with the planar design [19], and we suspect that this issue would be an advantage in order to avoid possible Si contamination which would be absent in our cells. In a recent paper on the study of the reversible operation of microtubular anode supported Ni–YSZ/YSZ/LSM–YSZ cells we reported that in electrolysis mode, the *j–V* curves showed a concave shape with the slope slightly increasing with current densities up to voltage values above 1.4 V where there was a tendency to saturation of the cell voltage [20]. We suspected that this effect was probably caused by the electroreduction of the YSZ electrolyte but this effect cannot completely explain all the cell behavior. In particular it cannot explain that the faradaic water reduction efficiency remains nearly 100% in the high current density region [21]. Thus, it has been suggested that similarly to the case of MIEC-type electrolytes increasing electronic conductivity also increases the oxygen electrode activity and reduces the overpotential. The effect is completely reversible except for severe electroreduction levels, where a permanent irreversible damage is observed. Similar effects were also reported by Schefold et al. [22]. The main objective of the present work is the understanding of the irreversible degradation that takes place at the YSZ electrolyte. The degradation was studied by AC impedance, SEM, EDX mapping and micro-Raman spectroscopy.

2. Experimental

Details of cell fabrication and microstructure, experimental setup for the electrolysis experiments, and information of the electrochemical studies performed to the cells can be found in Refs. [20,23].

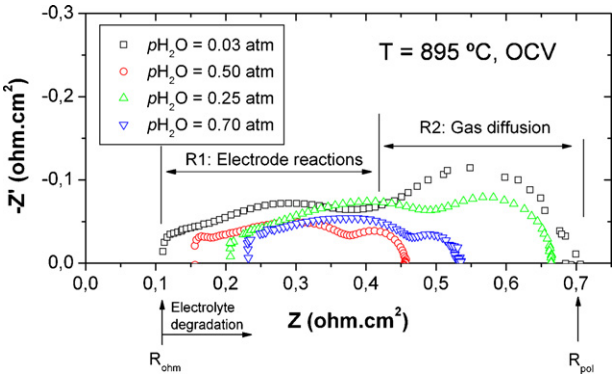

Fig. 1. AC impedance measurements recorded at OCV and 895 °C for the Ni–YSZ/YSZ/LSM–YSZ cell under different steam partial pressures.

Different sets of current density–voltage (*j–V*) experiments in both SOFC and SOEC mode were performed using the following growing sequence for pH_2O of 0.03, 0.50, 0.25 and 0.7 atm in the inner side (Ni/YSZ). For each steam composition we have measured at cell temperatures of 750, 820, 895 and 950 °C. The voltage range was taken between 0.5 and 2.5 V corresponding to density current values between −2.5 and 0.5 A cm^{-2}. Electrochemical impedance spectroscopy (EIS) was performed at OCV before and after all potentiodynamic experiments using an Autolab PGSTAT30 fitted with a frequency response analyser (FRA) (Autolab, Eco-Chemie, Netherlands), and using a sinusoidal signal amplitude of 100 mV over the frequency range of 10 kHz to 0.1 Hz. Details of the electrochemical results can be found in Ref. [20]. EIS at OCV was also analysed using the equivalent circuit composed of $LR_{ohm}(R_1Q_1)(R_2Q_2)$ where R_{ohm} represents the pure ohmic resistance. Each of the parallel circuits of resistance *R* and constant phase element *Q* gives account for its respective depressed semicircle going from high to low frequencies. A parasitic inductance *L* was added to account equipment contribution.

Scanning Electron Microscopy (SEM) experiments were performed under an accelerating voltage of 20 kV using a JEOL 6400 SEM (JEOL, Japan) fitted with Oxford Instruments INCA energy dispersive analytical system (EDS) for elemental X-ray analysis. The polished samples were also observed in a Field Emission-SEM (Nova NanoSEM, FEI, The Netherlands).

Micro-Raman measurements were performed in the backscattering configuration at room temperature (RT) in a DILOR XY spectrometer with a liquid-nitrogen-cooled charge coupled device (CCD) detector and excitation through the microscope. Laser excitation wavelength was chosen at $\lambda = 496.5$ nm to avoid the presence of narrow impurity emission bands presumably due to Er^{3+} impurity overlapping the Raman spectra when exciting with standard 514.5 Ar^+ ion laser beam. The Si mode at 520 cm^{-1} was used for frequency calibration. The spatial resolution was estimated to be about 2 μm^2.

3. Results and discussion

3.1. Effect of the degradation in the electrochemical behavior

AC impedance results measured at OCV and 895 °C, prior to each potentiodynamic measurement under different steam compositions are presented in Fig. 1. The experiment sequence is as given in the figure: 0.03, 0.50, 0.25 and 0.7 atm of pH_2O. The estimated experiment time was 10 min for each *j–V* measurement. As observed from the graph, there is a continuous increase of

Table 1
Resistance parameters obtained from the fittings for the AC impedance measurements shown in Fig. 1. The sequence shown in the table corresponds to the growing measured sequence.

pH_2O (atm)	R_{ohm} ($\Omega\,cm^2$)	R_1 ($\Omega\,cm^2$)	R_2 ($\Omega\,cm^2$)	R_{pol} ($\Omega\,cm^2$)	ASR ($\Omega\,cm^2$)
0.03	0.11	0.29	0.29	0.58	0.69
0.50	0.15	0.22	0.09	0.31	0.46
0.25	0.21	0.28	0.17	0.45	0.66
0.70	0.23	0.23	0.06	0.29	0.53

the ohmic resistance (high frequency cut off with *x*-axis) as we modified the steam composition. Since ohmic resistance does not depend on steam composition, the increase from 0.11 $\Omega\,cm^2$ to 0.23 $\Omega\,cm^2$ (as also observed in Table 1) is a consequence of cell degradation, possibly due to the operation under high current densities, as it will be further discussed.

AC impedance was also analysed using equivalent circuits. In Table 1 we summarize the different resistance components and ASR values obtained from the fitting of the AC impedance measurements to the equivalent circuit. It is observed that R_1 remains almost constant with operation time and with different steam concentrations. On the contrary, R_2 decreases when increasing the steam content in the inlet gas. From those observations, R_1 and R_2 were assigned to electrode reactions and gas diffusion, respectively.

Additional evidence of the YSZ degradation could be observed in Fig. 2(a). Using 70% of steam at 895 °C, at current densities above approximately −1.75 A cm^{-2}, a high scattering in the measured potential values is an indication of fast changes associated to the dynamics of YSZ electroreduction. The degradation is also illustrated when we observe the AC impedance data before and after this potentiodynamic experiment (Fig. 2(b)). Merely 10 min of operation under extreme conditions produce an irreversible damage causing a 63% increase of the ohmic resistance (from 0.23 $\Omega\,cm^2$ measured before the electrolysis operation to 0.37 $\Omega\,cm^2$ measured after the test), whereas the polarization contributions remain almost unaltered (0.31–0.32 $\Omega\,cm^2$).

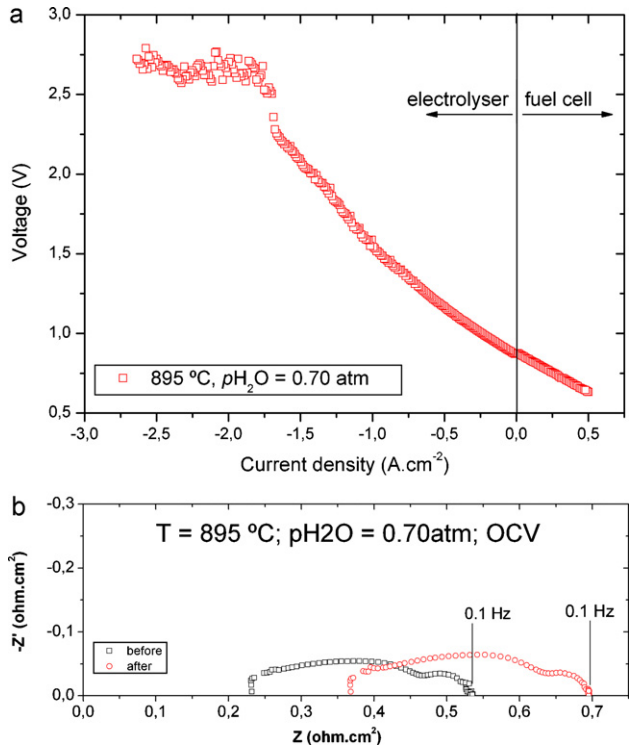

Fig. 2. (a) SOFC–SOEC experiments recorded at 70% steam concentration and 895 °C for the Ni–YSZ/YSZ/LSM–YSZ cell and (b) AC impedance measurements for the same cell before and after the electrochemical test.

3.2. Study of the degradation after cell operation

3.2.1. Microstructural studies

Microstructural studies of the operated cell using SEM experiments were performed. In Fig. 3 we present SEM images of transverse-cross sections of the cell after all the complete measurement cycles. Depending on the analysed zone, the cell presents different degrees of damage. In some regions of the cell we observed a clear indication of degradation of YSZ near to the air electrode side occurs. Fig. 3(a) presents the degradation at the earliest stage where large intergranular defects are observed near the oxygen electrode/electrolyte interface. Similar degradation was also reported by Knibbe et al. [18] when operating the cell at high current densities. These defects in the form of voids proliferate along the grain boundaries, as illustrated in Fig. 3(b). Fig. 3(c) and (d) presents regions of the cell where the degradation is more severe. The voids propagate through grain boundaries along the electrolyte and progress towards the hydrogen electrode side. In some cases this effect is accompanied with the delamination of the LSM/YSZ bilayer and even the rupture of the oxygen electrode, as shown in Fig. 3(d). The high internal oxygen partial pressures that take place at the oxygen electrode/electrolyte could be the origin for this degradation, as recently predicted by Virkar [17].

3.2.2. SEM-EDS elemental mapping and microanalysis

Cation diffusion at the oxygen electrode has been previously reported in SOEC cells as a sign of degradation [14]. In order to study the possible diffusion of species within the oxygen electrode/electrolyte and electrolyte/hydrogen-steam electrode in our microtubular cells, SEM-EDS elemental mapping for Zr, Y, Ni, La and Mn ions was performed. From the results shown in Fig. 4, we can conclude that Ni, La and Mn are limited to the electrode region so there is no evident cation diffusion of species between the different cell layers.

EDS microanalysis was also performed, especially in the electrolyte region, were we have observed signs of degradation. In Fig. 5, we present two SEM micrographs that correspond to the analysed area for a blank sample (a) and for the degraded sample (b). The measured oxygen fraction versus the total amount of analysed atoms, Zr, Y and O (atomic %) as a function of the distance to the oxygen electrode is also shown in this figure for both the untreated blank sample that serves as standard reference, and for the degraded sample. Although we expect some error in the quantitative determination of atomic fractions mainly because of the presence of pores which changes the density of the explored layer, we can extract some qualitative but valuable information. It is clear that the oxygen content along the YSZ electrolyte varies almost linearly from low oxygen values near the water electrode to higher values near to oxygen electrode. This is again consistent with the predictions of Virkar and the observations of other authors as discussed in Section 1. The decrease of atomic oxygen at the water electrode is presumably due to electroreduction of the YSZ layer.

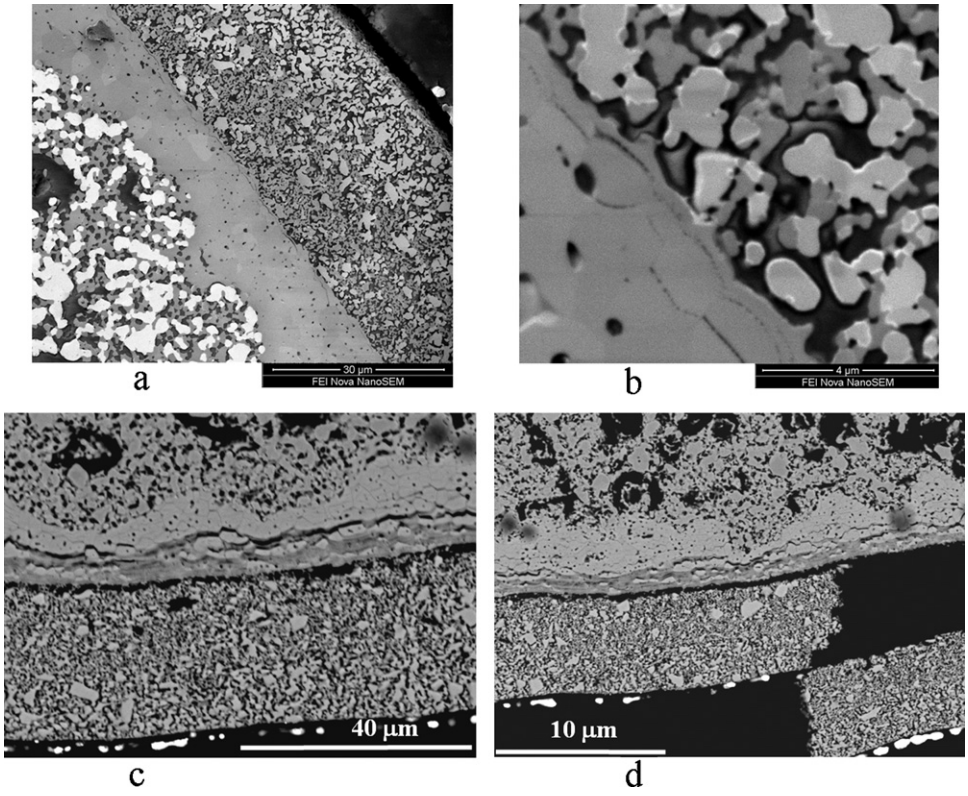

Fig. 3. SEM micrographs showing different stages of damage for the same cell (a) general view of the cell; (b) origin of the degradation at the YSZ grain boundaries; (c) cracking of the YSZ electrolyte and (d) delamination of the LSM–YSZ electrode.

This increase is accompanied by an increase of the oxygen partial pressure at the oxygen electrode/electrolyte. In addition, we observed that near to the oxygen electrode/electrolyte interface the oxygen tends to accumulate in pores or voids, where we can also observe severe cracking. This is also coherent with the work of Knibbe et al. [18]. They performed EDXS analysis (TEM) across the grain boundary and observed that there is an increase of oxygen at the porous region near the oxygen electrode. They conclude that at high current densities in SOEC mode, there is an increase of the electromotive potential in the YSZ electrolyte adjacent to the oxygen electrode, which allows the formation of oxygen at the YSZ grain boundaries close to the oxygen electrode.

3.2.3. Raman studies

Raman spectroscopy is a common technique to study aging and thermal evolution of doped zirconia [24]. In this case, we have

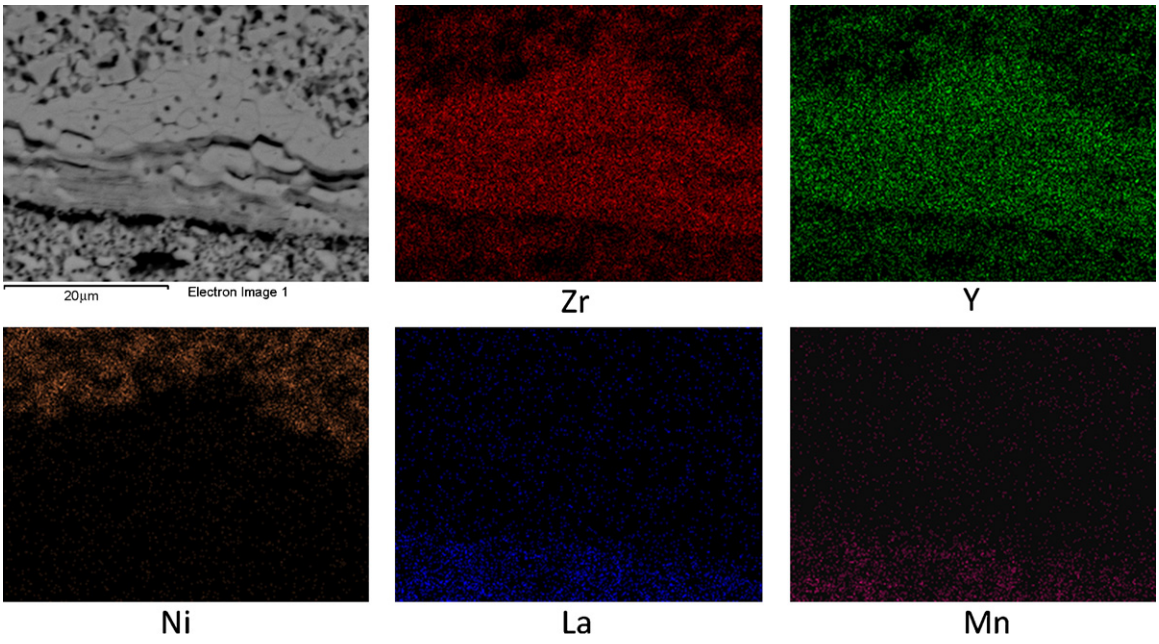

Fig. 4. Elemental mapping for Ni, Zr, Y, La and Mn for the analysed region.

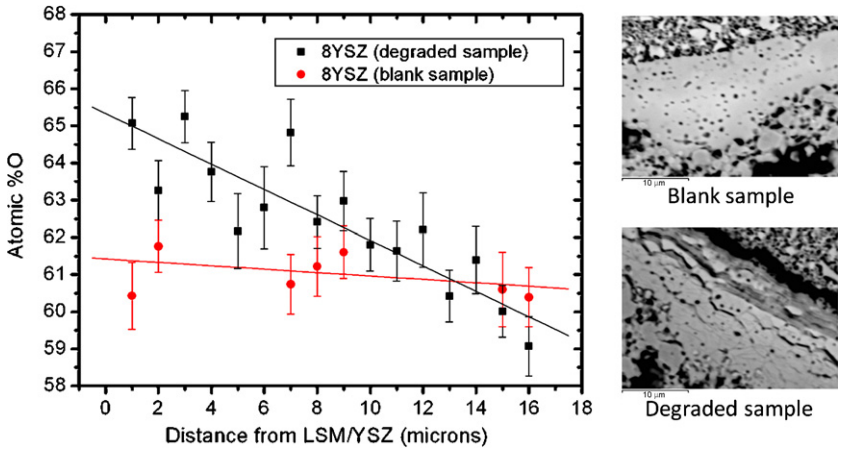

Fig. 5. Oxygen atomic content along the YSZ electrolyte measured by EDS. As standard reference, oxygen content of a reference cell is also plotted in the graph. SEM micrographs for the analysed regions are also shown.

performed micro-Raman studies along the YSZ electrolyte. The SEM micrograph from Fig. 6 corresponds to the analysed zone. We have recorded Raman spectra along the thickness of the YSZ electrolyte every 2 μm. The characteristic vibrational Raman spectra are shown in Fig. 6. The black spectrum from the figure corresponds to an untreated blank sample, which is shown for comparison. The Raman spectra measured along the electrolyte thickness do not show any apparent difference with that of the untreated sample except in the very near region to the oxygen electrode. This spectrum presents an intense band centred at around 620 cm^{-1} which corresponds to the cubic phase of the zirconia. The absence of the otherwise noticeable 260 cm^{-1} mode eliminates the presence of tetragonal phase unless in large amounts. However, when we analyse the region adjacent to the oxygen electrode (from a distance of 0 to 4 μm from interface), the 620 cm^{-1} band broadens and also moves to lower wavelength (centred at around 610 cm^{-1}). Band widening is often associated in Raman spectroscopy with structural disorder. We do not clearly understand if this is here the case, but the band widening could be again related with the increase of oxygen observed by EDX at the YSZ grain boundaries close to the oxygen electrode. Micro-Raman spectroscopy could be in this way also a tool to study the degradation in the region close to the oxygen electrode interface although we did not observe any phase change of the YSZ in this region.

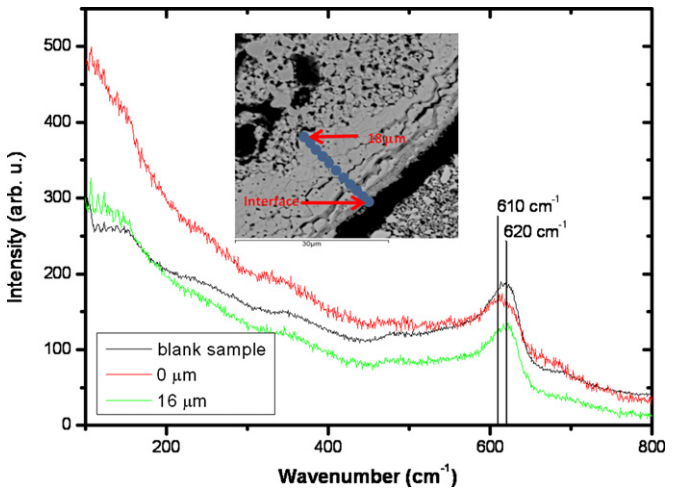

Fig. 6. Raman spectra along the YSZ electrolyte. Raman spectrum of a blank sample is also shown for comparison. The inset shows a SEM micrograph for the analysed region.

4. Conclusions

Operation of anode supported YSZ-based microtubular cells in SOEC mode under high voltages (>1.8 V) produces irreversible degradation of the electrolyte, caused by YSZ electroreduction. Voids were detected at the grain boundaries of the YSZ in the region adjacent to the oxygen electrode. In the most degraded cell regions these voids progress along the grain boundaries generating cracks in the electrolyte. The presence of oxygen in excess near to oxygen electrode degraded regions as well as the depletion of oxygen in the near to water electrode regions, is associated with the high pO_2 at the electrolyte–electrode interface, and it is also in concordance with Virkar model for the redistribution of oxygen along the thin YSZ electrolyte. This effect also produces delamination of the O_2 electrode, as it was also observed and thus, the degradation produces an increase in the cell impedance.

References

[1] E. Erdle, et al., Proceedings of the Third International Workshop, vol. 2, High Temperature Technology and its Applications, Konstanz, Federal Republic of Germany, 1986, pp. 727–736.
[2] R. Rivera-Tinoco, C. Mansilla, C. Bouallou, Energy Convers. Manage. 51 (2010) 2623–2634.
[3] A. Hauch, S.H. Jensen, S. Ramousse, M. Mogensen, J. Electrochem. Soc. 153 (9) (2006) A1741–A1747.
[4] G. Schiller, A. Ansar, M. Lang, O. Patz, J. Appl. Electrochem. 39 (2009) 293–301.
[5] S. Elangovan, J.J. Hartvigsen, L.J. Frost, Int. J. Appl. Ceram. Technol. 4 (2007) 109–118.
[6] M.A. Laguna-Bercero, S.J. Skinner, J.A. Kilner, J. Power Sources 192 (2009) 126–131.
[7] S. Pati, K.J. Joon, S. Gopalan, U.B. Pal, J. Electrochem. Soc. 156 (2009) B1067–B1077.
[8] T. Ishihara, N. Jirathiwathanakul, H. Zhong, Energy Environ. Sci. 3 (2010) 665–672.
[9] A. Brisse, J. Schefold, M. Zahid, Int. J. Hydrogen Energy 33 (2008) 5375–5382.
[10] J. Hartvigsen, S. Elangovan, L. Frost, A. Nickens, C. Stoots, J. O'Brein, J.S. Herring, Carbon dioxide reduction, Metallurgy (2008) 171–182.
[11] Z. Zhan, W. Kobsiriphat, J.R. Wilson, M. Pillai, I. Kim, S.A. Barnett, Energy Fuels 23 (2009) 3089–3096.
[12] C. Graves, S.D. Ebbesen, M. Mogensen, Solid State Ionics, (2010) doi:10.1016/j.ssi.2010.06.014.
[13] A. Hauch, S.D. Ebbesen, S.H. Jensen, M. Mogensen, J. Electrochem. Soc. 155 (2008) B1184–B1193.
[14] M.S. Sohal, J.E. O'Brien, C.M. Stoots, V.I. Sharma, B. Yildiz, A. Virkar, Proceedings of the ASME FUELCELL, 2010, pp. 1–11.
[15] A. Momma, T. Kato, Y. Kaga, S. Nagata, J. Ceram. Soc. Jpn. 105 (1997) 369–373.
[16] J.R. Mawdsley, J.D. Carter, A.J. Kropf, B. Yildiz, V.A. Maroni, Int. J. Hydrogen Energy 34 (34) (2009) 4198–4207.
[17] A.V. Virkar, Int. J. Hydrogen Energy 35 (2010) 9527–9543.
[18] R. Knibbe, M.L. Traulsen, A. Hauch, S.D. Ebbesen, M. Mogensen, J. Electrochem. Soc. 157 (2010) B1209–B1217.
[19] K. Kendall, Int. Appl. Ceram. Technol. 7 (2010) 1–9.

[20] M.A. Laguna-Bercero, R. Campana, A. Larrea, J.A. Kilner, V.M. Orera, Fuel Cells (2010) 1–8, doi:10.1002/fuce.201000069.
[21] M.A. Laguna-Bercero, R. Campana, A. Larrea, J.A. Kilner, V.M. Orera, J. Electrochem. Soc. 6 (2010) B852–B855.
[22] J. Schefold, A. Brisse, M. Zahid, J. Electrochem. Soc. 159 (2009) B897–B904.
[23] R. Campana, R.I. Merino, A. Larrea, I. Villarreal, V.M. Orera, J. Power Sources 192 (2009) 120–125.
[24] K. Nomura, Y. Mizutani, M. Kawai, Y. Nakamura, O. Yamamoto, Solid State Ionics 132 (2000) 235–239.